Journal of Alloys and Compounds 858 (2021) 158229

Contents lists available at ScienceDirect

Journal of Alloys and Compounds

journal homepage: www.elsevier.com/locate/jalcom

High-temperature thermochemical energy storage using metal hydrides: Destabilisation of calcium hydride with silicon

Arnaud C.M. Griffond[a], M. Veronica Sofianos[a,b,*], Drew A. Sheppard[a], Terry D. Humphries[a], Anna-Lisa Sargent[c], Martin Dornheim[c], Kondo-Francois Aguey-Zinsou[d], Craig E. Buckley[a]

[a] Physics and Astronomy, Fuels and Energy Technology Institute, Curtin University, GPO Box U1987, Perth, WA 6845, Australia
[b] School of Chemical and Bioprocess Engineering, University College Dublin, Belfield, Dublin 4, Ireland
[c] Department of Nanotechnology, Institute of Materials Research, Helmholtz-Zentrum Geesthacht, Max-Planck-Strasse 1, 21502 Geesthacht, Germany
[d] Merlin Group, School of Chemical Engineering, The University of New South Wales, Sydney, NSW 2052, Australia

ARTICLE INFO

Article history:
Received 22 September 2020
Received in revised form 1 December 2020
Accepted 6 December 2020
Available online 10 December 2020

Keywords:
Metal hydride
Thermal energy storage
Calcium hydride
Thermodynamics
Destabilisation

ABSTRACT

The thermochemical energy storage properties of calcium hydride (CaH_2) destabilised with either silicon (Si) or Ca_xSi_y compounds at various molar ratios, were thoroughly studied by a combination of experimental and computer assisted thermodynamic calculations. Particularly, the destabilisation effect of Si on CaH_2 at five different molar ratios (1:1, 1:2, 2:1, 3:4, 5:3 CaH_2 to Si) was extensively investigated. Theoretical calculations predicted a multi-step thermal decomposition reaction between CaH_2 and Si forming Ca_xSi_y at varying temperatures, which was confirmed by *in-situ* synchrotron X-ray diffraction, differential scanning calorimetry, thermogravimetric analysis and mass-spectroscopic measurements. The most suitable destabilisation reactions between CaH_2 and Si or Ca_xSi_y that meet the criteria of a thermal energy storage system for the next-generation of concentrated solar power (CSP) plants were identified. The CaH_2 and CaSi system (in a 2:3 molar ratio of CaH_2 to CaSi) showed desirable operating conditions with a decomposition temperature of 747 ± 33 °C at a hydrogen pressure of 1 bar. Pressure composition isothermal measurements were conducted on this system to determine its practical enthalpy of decomposition to form Ca_5Si_3. The calculated value (107.3 kJ mol^{-1} H_2) was lower compared to the experimentally determined value (154 ± 4 kJ mol^{-1} H_2). This mismatch was mainly due to the formation of CaO and a CaSi solid solution in addition to the desired Ca_5Si_3 phase.

1. Introduction

A transition towards the use of green energy sources that are based on renewable energy production instead of fossil fuels, has recently been globally recognised. Even though a combination of renewable energy sources will be required to attain the base-load power needed to cover the worlds energy demand, solar energy is the most promising for a long-term solution [1]. Specifically, our planet receives more than 5000 times the current world's energy requirements through incident sunlight, while all energy from other renewable energy sources combined totals less than 1% of solar [1]. According to Abbot, if we consider only the solar power received at the desert regions of our planet, all other renewable sources combined would still only produce less than 3% of that of solar power [1].

One method of utilising solar power for electricity production is concentrating solar power (CSP). The market for CSP has gained interest over the years and currently there are over 180 commercial projects either operational, under construction or under development [2]. This is due to its high efficiency and unlike photovoltaic energy, diverse solutions are available to store thermal energy in comparison to electrical energy [3]. Its operating principal is based on focusing incident sunlight using curved mirrors to generate heat that is then used to create superheated steam. This steam is then used to produce electricity *via* a turbine [4–6]. The major drawback of solar energy is its intermittent supply. This is due to daily and seasonal variation in solar radiation, and unpredictable weather conditions. To counteract the existing mismatch between the discontinuous solar energy supply and electricity consumption, the implementation of a thermal energy storage (TES) system into CSP plants is required [7].

Currently there are three basic types of TES systems which are based on the: (1) sensible heat of materials [7,8]; (2) latent heat of fusion [9,10] and (3) thermochemical heat produced during chemical

* Corresponding author at: School of Chemical and Bioprocess Engineering, University College Dublin, Belfield, Dublin 4, Ireland.
E-mail address: mvsofianou@gmail.com (M.V. Sofianos).

https://doi.org/10.1016/j.jallcom.2020.158229
0925-8388/

reactions [11–22]. Most of the current CSP systems with TES systems use a molten salt mixture as sensible heat storage [23]. The working principle of the molten salt TES systems is simply based on using the heat capacity of the mixture to store energy as a function of temperature. Another solution is to use the energy released during a first-order phase transition of a material that is at a constant temperature (latent heat). These materials are also called Phase Change Materials (PCMs). Thermochemical heat storage, is based on reversible chemical reactions. The solar heat collected is used to drive an endothermic reaction, its temperature and pressure at which this reaction occurs is directly linked to its reaction enthalpy and entropy [24]. During the daytime, a thermochemical reaction takes place while heat is absorbed (endothermic reaction), whereas at night the reverse reaction occurs, and heat is released (exothermic reaction). Metal hydrides are of particular interest as thermochemical materials due to their high enthalpy of hydrogen absorption (*e.g.* 189.2 kJ mol^{-1} H_2 at 1 bar equilibrium pressure for CaH_2) [12,20,21]. A hydrogen storage unit is required to store the hydrogen desorbed from the metal hydride during the endothermic reaction (charging of the TES system) when using metal hydrides for thermochemical energy storage. This unit can either be a gas storage container or a low temperature metal hydride (LTMH) that can store the hydrogen released from the high-temperature metal hydride (HTMH) [25]. Hydrogen moves between the storage and the HTMH unit according to temperature or pressure change generated after heating or cooling the system [26].

Metal hydrides are promising TES systems due to their high energy density that can be 10 times higher than the commercially used molten salts in current CSP plants [20,21]. One of the main disadvantages of using a molten salt TES system for CSP applications is their limited maximum operating temperature (< 565 °C) [27]. If a higher temperature range could be attained, a higher efficiency of the CSP system would be achieved. Specifically, by raising the temperature to between 600 and 800 °C, the power cycle efficiency would increase by 50% in comparison to the existing ones while the cost would be reduced by 40% [28]. A number of metal hydrides possess suitable thermodynamic properties that make them able to absorb and desorb hydrogen at high temperature at moderate pressures (> 600 °C, < 10 bar) [20,21,29].

Corgnale et al. calculated that CaH_2 paired with TiFe is the most economically viable solution for HTMH/LTMH storage that works well at low pressures and high temperatures (between 800 and 1000 °C) and approaches the DOE economic target for TES systems of \$15/kWh_{th} [26]. A comprehensive study comparing molten salts and several metal hydrides by Manickam et al., detailed that CaH_2 has a favourable practical (85% of theoretical) energy density of 4198 kJ kg^{-1} at operating conditions of 1000 °C and 1.2 bar of H_2 pressure [21].

The abundance and low cost of calcium makes calcium hydride an interesting candidate as a HTMH. Unfortunately, its decomposition temperature is too high for both current and next-generation of CSP plants. Additionally, even if these operating conditions were possible for CSP plants, both calcium hydride (melting point = 983 °C) and calcium metal (melting point = 842 °C) would be corrosive liquids [30–32], which in turn would require specialised and expensive engineering for containment vessels.

By adding metallic elements or an alloy (M) to calcium hydride, the thermal desorption pathway may be altered from Eqs. (1) and (2). In this situation, the Gibbs free energy of reaction decreases with an associated decrease in the desorption temperature. This process was studied by Vajo et al. and it is known as thermodynamic destabilisation [33].

$$CaH_2 \rightleftharpoons Ca + H_2 \quad (1)$$

$$xCaH_2 + yM \rightleftharpoons Ca_xM_y + xH_2 \quad (2)$$

This approach was successfully applied by Veleckis et al. while it was theoretically studied by Vajo [33,34]. In the study by Veleckis et al., CaH_2 was destabilised by the addition of Al and a multistep desorption reaction was observed as seen in Eqs. (3) and (4):

$$CaH_2 + 4Al \rightleftharpoons Al_4Ca + H_2 \quad (3)$$

$$CaH_2 + Al_4Ca \rightleftharpoons 2Al_2Ca + H_2 \quad (4)$$

The reaction between CaH_2 and Al occurs at 1 bar of H_2 pressure at 414 °C with an enthalpy of reaction $\Delta H \approx 74$ kJ mol^{-1} H_2 [34]. The Al_4Ca phase then reacts with the excess CaH_2 to form Al_2Ca (Eq. (4), $T_{1\ bar} \approx 480$ °C, $\Delta H \approx 83.1$ kJ mol^{-1} H_2). Ward et al. recently advanced this study on the $CaAl_2$ system by extending the operational temperatures for TES applications to 600 °C, operating at ~23 bar of H_2 pressure, exhibiting a 1.9 wt% H_2 capacity [35]. The system was cycled 100 times with no significant loss of hydrogen capacity. The main limitation of this system is its high operating pressure (~23 bar of H_2 pressure), which increases the engineering costs of the TES system and also exceeds the targets of the US DoE Sunshot programme [27]. Overall the aim is to manufacture a complete TES system (including the cost of the hydrogen storage unit, engineering costs and heat transfer system) that produces energy at a cost of below \$15/kWh_{th}.

In 1921, Wohler et al. were the first to use CaH_2 instead of pure Ca to form calcium monosilicide (CaSi), which allowed formation of calcium disilicide at a lower temperature [36]. It was also demonstrated that formation of calcium disilicide ($CaSi_2$) was thermodynamically preferable during the reaction. In addition, for a 1:1 molar ratio of CaH_2: Si, a two-step reaction took place. First $CaSi_2$ was formed from the reaction between CaH_2 with Si, before further reaction with the excess CaH_2 present in the system to form CaSi. Since then, several studies have focused on the hydrogen storage properties of the calcium silicon system with different Ca_xSi_y phases being observed. Anikina et al. studied the hydrogen sorption properties of calcium silicide, and determined the enthalpy and entropy of the CaSi–H_2 system during desorption to be ΔH_{des} = 53.7 ± 1.2 kJ mol^{-1} H_2 and ΔS_{des} = 94.2 ± 2.7 J mol^{-1} H_2. K^{-1}) [37]. Wu et al. studied the Ca_5Si_3 and Ca_2Si structures and their hydrogen storage properties at low temperatures and high pressures [38,39]. They showed that at high temperatures, the sample disproportionately transforms into a mixture of crystalline CaH_2 and other calcium silicide phases.

To the best of our knowledge, this is the first study to present a combination of theoretical and experimental thermodynamic calculations identifying the most suitable destabilisation reactions between CaH_2 and Si or Ca_xSi_y compounds; that meet the required operating temperature range (600–800 °C) of the next-generation CSP plants. The most promising theoretically calculated reactions were experimentally explored in order to optimise the thermodynamic properties and also the reversible formation of the reactants. *In-situ* synchrotron X-ray diffraction measurements were performed while heating to identify the exact reaction pathways that take place at various temperatures. The calculated thermodynamic predictions were compared with the obtained experimental data using hydrogen sorption measurements.

2. Materials and methods

2.1. Theoretical thermodynamic calculations

Chemical reactions between Ca, Si and the Ca_xSi_y phases were simulated by compiling known thermodynamic data, such as enthalpy (ΔH), entropy (ΔS) and Gibbs free energy (ΔG), using the HSC software [40]. The method applied did not take into account kinetic models, flow and heat transfer. A database of the thermodynamic data for the Ca–Si–H system was compiled by searching the available literature. Data for pure elements were collected from Dinsdale et al. and Binnewise et al. [41,42]. The thermodynamic data of all the

calcium-silicon compounds; Ca_2Si, Ca_5Si_3, CaSi, Ca_3Si_4, $Ca_{14}Si_{19}$ and $CaSi_2$, were defined by Heyrman et al. [43]. In this case, ΔG is expressed as a function of temperature. The quantity of heat released per mole of hydrogen absorbed for each reaction was also calculated according to its temperature dependence. The equilibrium pressure for each reaction was also determined according to Eq. (5) for the desired temperature range (600–800 °C).

$$\Delta G_{RXN} = RT \ln (P/P_0) \quad (5)$$

Where, R is the ideal gas constant (8.3144 J K^{-1} mol^{-1}), T is the temperature that the reaction takes place (K), P is the associated hydrogen gas pressure (bar) and P_0 = 1 bar.

2.2. Sample preparation

All air and moisture sensitive chemicals were handled in an argon filled glovebox (mBraun, Germany) with less than 1 ppm of H_2O and O_2, as to avoid any sample contamination. Calcium hydride was synthesised by hydrogenating pure Ca (99%, Sigma Aldrich) by the following method. A stainless-steel reactor was filled with pure Ca before being heated to 360 °C at a ramp rate of 10 °C/min while under dynamic vacuum. The hydrogenation of Ca was then conducted at 450 °C at an initial 20 bar of H_2 pressure. When the pressure equalled 1 bar, the reactor was re-filled with hydrogen. The absorption reaction was considered complete when the pressure stabilised at a pressure > 1 bar. The reactor temperature was then raised to 480 °C while under 10 bar of H_2 to ensure complete hydrogenation had occurred.

The as-prepared CaH_2 was then ball milled with Si (99%, Sigma Aldrich) at five different molar ratios (1:1, 1:2, 2:1, 3:4, 5:3 CaH_2 to Si) using an Across International Planetary Ball Mill (PQ-N04) employing tempered steel vials (50 mL capacity) and balls under an argon atmosphere at room temperature. The ball to powder mass ratio was 20:1 (equal amounts of 6 mm Ø and 10 mm Ø balls) and the total ball milling time was 3 h at 400 rpm with 35 bi-rotational cycles applied for 5 min each.

2.3. Sample characterisation

All samples were analysed before and after their thermal analysis by *ex-situ* powder X-ray diffraction (XRD) using a Bruker D8 Advance diffractometer (Cu–Ka radiation) using an airtight sample holder covered with a poly(methylmethacrylate) (PMMA) dome to prevent oxygen/moisture contamination during data collection. The PMMA dome resulted in a broad hump in the XRD patterns centred at ~ 20° 2θ, where 2θ is the scattering angle. In order to minimise the hump and maximise the diffraction peak, the variable divergence slit (VDS) was set at 6 mm. This resulted in the beam size not being angle dependent and therefore fixed at a constant position on the sample, ensuring better statistics even when a small amount of material was used. Diffraction patterns were quantitatively analysed *via* the Rietveld method [44] using TOPAS software (Bruker-AXS).

Temperature programmed desorption (TPD) and pressure composition isothermal (PCI) measurements were undertaken on all samples using a computer-controlled Sieverts/volumetric apparatus [45]. TPD measurements were conducted from room temperature up to 750 °C, whereas PCI measurements were conducted at a range of temperatures between 698 °C and 778 °C. The step size during the PCI measurements was 2 bar and each step was 5 h in total with samples sizes of 0.5–0.7 g. All samples were heated at a ramp rate of 5 °C/min. The precision and accuracy of the digital pressure transducer (Rosemount 3051S) was 14 mbar. Room temperature measurements were recorded using a 4-wire platinum resistance temperature detector (RTD), while the sample temperature was monitored using a K-type thermocouple.

For the TPD measurements, the stainless steel sample holders were placed in an aluminium coated stainless steel reactor to avoid hydrogen permeation through the stainless steel at high temperature [46]. The stainless steel endcap was not aluminium coated due to limitations of the coating method, and as such a correction for hydrogen permeation was applied to all data [45]. A silicon carbide (SiC) sample holder was used during the PCI measurements, where the SiC tube was connected to the Sievert's apparatus using Swagelok tube fittings and a Teflon ferrule [46]. Hydrogen does not permeate through SiC vessels at high temperatures removing the necessity for data correction.

Differential scanning calorimetry (DSC), thermogravimetric analysis (TGA) and mass spectrometry (MS) measurements were performed simultaneously under an argon flow of 20 mL/min using a Mettler Toledo TGA/DSC 1 coupled with an Omnistar MS. The instrument was located inside argon filled gloveboxes as to minimise air/moisture contamination of the samples during data collection. The samples were placed inside alumina crucibles and heated at a ramp rate of 10 °C/min from room temperature to 900 °C. The TGA/DSC was calibrated in temperature and enthalpy by using the following reference materials: In, Zn, Al and Au.

In-situ synchrotron X-ray diffraction (SR-XRD, λ = 0.59027 Å) was performed at the Australian Synchrotron in Melbourne, Australia [47]. Data was collected using a Mythen microstrip detector using an exposure time of 30 s [48]. Samples were loaded in quartz capillaries (outer diameter 0.7 mm, wall thickness 0.01 mm) and mounted in a sample holder made from Swagelok fittings, in a glove box filled with purified argon (< 1 ppm O_2 and H_2O). The sample holder was then connected to a hydrogen gas filling/vacuum manifold, placed under a H_2 back-pressure of 1.5 bar and the capillary heated at a rate of 10 °C/min from room temperature to 886 °C and cooling ramp down to 338 °C using a hot air blower. The temperature of the hot air blower was calibrated against the known thermal expansion coefficient of NaCl and Ag [49–51].

3. Results and discussion

3.1. Thermodynamic predictions

Thermodynamic predictions of the reactions between CaH_2 and Si or Ca_xSi_y phases were derived from the Ca–Si phase diagram [52], which take place at the lowest temperature of reaction and at 1 bar of H_2, and are presented in Table 1. The calculated predictions helped to identify the most suitable destabilisation reaction for CaH_2 that would meet Sunshot's targets for TES systems [27]. It can be seen that reacting CaH_2 and Si in varying molar ratios will form a variety of Ca_xSi_y compounds and also release H_2 in the process. In Table 1, the thermodynamically preferable reaction between CaH_2 and Si can be determined comparing reaction (RXN) 1–6. RXN 4 (Table 1) has the lowest enthalpy of reaction *i.e.* a lower demand in energy and a lower temperature of reaction ($T_{1\,bar}$) resulting in the formation of Ca_3Si_4 and release of hydrogen at 381 °C, while RXN 3 would release hydrogen at 571 °C. The reactions between $CaSi_2$ and CaH_2 are described using RXNs 7–11 (Table 1) with RXN 9 having the lowest enthalpy of reaction of 81.2 kJ/mol H_2 ($T_{1\,bar}$ = 405 °C) while RXN 8 would release hydrogen at 640 °C.

Surveying the reactions between CaH_2 and CaSi (1:1 and 2:3, RXNS 15–16), it can be seen that both of these reactions would result in a $T_{1\,bar}$ occurring in the range of temperature required for application of between 600 and 800 °C. In fact, RXN 16 from Table 1 is predicted to have a $T_{1\,bar}$ = 703 °C, releasing up to 1.4 wt% of hydrogen and resulting in a gravimetric energy density of 743.4 kJ kg^{-1}.

From all 21 predicted decomposition reactions between various ratios of CaH_2 and Si or Ca_xSi_y, it can be seen that each of the Ca_xSi_y reagents used in RXNS 7–21 can be synthesised using the products of RXNS 1, 2, 4, 5 and 6 along with additional CaH_2. As such, to

Table 1
Thermodynamic predictions of the decomposition reactions between CaH_2 and Si or Ca_xSi_y: temperature of reaction at 1 bar H_2 back pressure, enthalpy of reaction per mole of H_2 released, gravimetric energy density and weight percent of H_2 released by reaction.

Reaction No.	Reaction	Temperature T_{RXN} (°C)	Enthalpy ΔH (kJ mol^{-1} H_2)	Gravimetric Energy Density at T_{RXN} (kJ kg^{-1})	H_2 (wt%)
	Si				
1	$CaH_2 + Si \rightleftharpoons CaSi + H_2$	413	89.3	1272	2.87
2	$CaH_2 + 2Si \rightleftharpoons CaSi_2 + H_2$	370	83.4	849	2.05
3	$2CaH_2 + Si \rightleftharpoons Ca_2Si + 2H_2$	571	103.9	1852	3.59
4	$3CaH_2 + 4Si \rightleftharpoons Ca_3Si_4 + 3H_2$	381	82.7	1040	2.53
5	$5CaH_2 + 3Si \rightleftharpoons Ca_5Si_3 + 5H_2$	520	96	1629	3.42
6	$14CaH_2 + 19Si \rightleftharpoons Ca_{14}Si_{19} + 14H_2$	391	85.8	1070	2.51
	$CaSi_2$				
7	$CaH_2 + CaSi_2 \rightleftharpoons 2CaSi + H_2$	455	94	680	1.46
8	$3CaH_2 + CaSi_2 \rightleftharpoons 2Ca_2Si + 3H_2$	640	110.6	1518	2.72
9	$CaH_2 + 2CaSi_2 \rightleftharpoons Ca_3Si_4 + H_2$	405	81.2	346	0.86
10	$7CaH_2 + 3CaSi_2 \rightleftharpoons 2Ca_5Si_3 + 7H_2$	587	101.4	1217	2.42
11	$9CaH_2 + 19CaSi_2 \rightleftharpoons 2Ca_{14}Si_{19} + 9H_2$	435	90.8	370	0.82
	Ca_3Si_4				
12	$CaH_2 + Ca_3Si_4 \rightleftarrows 4CaSi + H_2$	496	107.5	391	0.73
13	$5CaH_2 + Ca_3Si_4 \rightleftarrows 4Ca_2Si + 5H_2$	684	116.3	1313	2.28
14	$11CaH_2 + 3Ca_3Si_4 = 4Ca_5Si_3 + 11H_2$	636	106.8	1012	1.91
	CaSi				
15	$CaH_2 + CaSi \rightleftharpoons Ca_2Si + H_2$	741	118.4	1074.1	1.83
16	$2CaH_2 + 3CaSi \rightleftharpoons Ca_5Si_3 + 2H_2$	703	107.3	743.4	1.40
	Ca_5Si_3				
17	$CaH_2 + Ca_5Si_3 \rightleftharpoons 3Ca_2Si + H_2$	803	142.3	436	0.62
	$Ca_{14}Si_{19}$				
18	$5CaH_2 + Ca_{14}Si_{19} \rightleftharpoons 19CaSi + 5H_2$	471	97.7	374	0.77
19	$24CaH_2 + Ca_{14}Si_{19} \rightleftharpoons 19Ca_2Si + 24H_2$	679	114.2	1302	2.30
20	$CaH_2 + 4Ca_{14}Si_{19} \rightleftharpoons 19Ca_3Si_4 + H_2$	1507	−90.4	−20	0.05
21	$53CaH_2 + 3Ca_{14}Si_{19} \rightleftharpoons 19Ca_5Si_3 + 53H_2$	629	104.1	1000	1.94

determine the accuracy of the theoretical predictions, RXNS 1–5 where initially chosen to be tested experimentally to determine their precise thermal decomposition pathways and the temperatures at which they occurred. The reactions chosen for this study have CaH_2 to Si molar ratios of 1:1, 1:2, 2:1, 3:4 and 5:3.

3.2. Thermal analysis

Temperature programmed desorption (TPD) measurements were performed from room temperature up to 750 °C on the selected five ratios of CaH_2 and Si (Ca:Si; 1:1, 1:2, 2:1, 3:4 and 5:3) to determine the thermal decomposition pathways of each mixture and the experimental gravimetric hydrogen content. The experimental wt% presented in Table 2 were then compared to the theoretical wt% values obtained from HSC (RXNS 1–5, Table 1).

It is evident that the experimental values of the desorbed hydrogen are lower than the theoretical values for all five samples. This is a very common phenomenon and is mostly due to the following reasons. Either the sample is not pure (in this particular case CaO is an impurity in all studied CaH_2 and Si systems), therefore the theoretical value does not match the experimental, or during desorption, the equilibrium pressure of that particular reaction was reached and the reaction stopped before completion (this is the case for Samples 3 and 5).

Ex-situ XRD was conducted on all five samples before (Fig. S1) and after their TPD measurements (Fig. 1). *Ex-situ* XRD on the

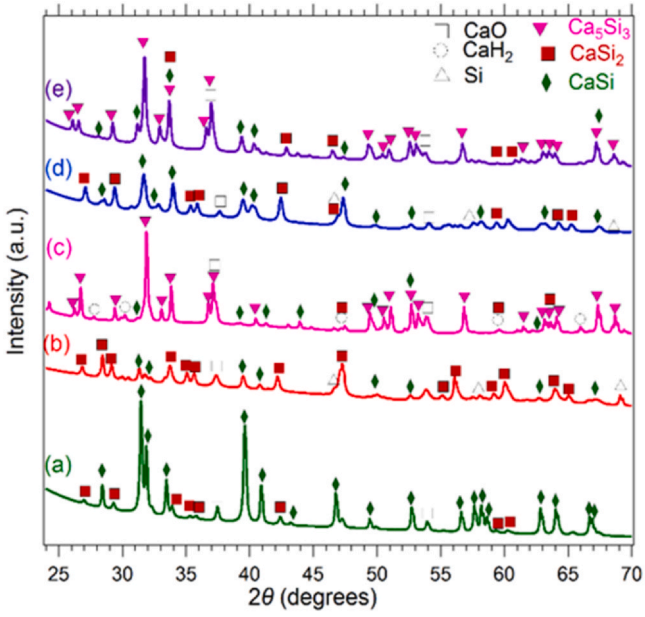

Fig. 1. *Ex-situ* X-ray powder diffraction patterns of CaH_2 and Si with (a) 1:1, (b) 1:2, (c) 2:1, (d) 3:4 and (e) 5:3 molar ratios after temperature programmed desorption (TPD) measurements.

Table 2
Theoretical and experimental (TPD) values of the hydrogen content (H_2 wt%) for five different molar ratios of CaH_2 and Si. The decomposition products of each system and their quantities determined by quantitative XRD analysis are presented.

Sample no.	System	Ratio	Theoretical H_2 wt%	Experimental H_2 wt%	Si wt%	CaH_2 wt%	CaO wt%	CaSi wt%	$CaSi_2$ wt%	Ca_5Si_3 wt%
1	$CaH_2 + Si$	1:1	2.87	2.73	0	0	4	89	7	0
2	$CaH_2 + 2Si$	1:2	2.05	1.89	13	0	8	5	74	0
3	$2CaH_2 + Si$	2:1	3.59	3.00	0	6	10	6	0	79
4	$3CaH_2 + 4Si$	3:4	2.53	2.41	1	0	5	45	49	0
5	$5CaH_2 + 3Si$	5:3	3.42	2.98	0	0	12	54	9	25

as-prepared samples (Fig. S1) confirmed that CaH_2 does not react with Si during ball milling to form a Ca–Si phase. The obtained powder diffraction patterns after their TPD measurements (Fig. 1) aided the identification of the decomposition products. Quantitative Rietveld analysis was performed on the obtained XRD patterns, with data presented in Table 2. CaO is identified in all samples and it is due to contamination of the starting material (CaH_2) and sample handling.

For the 1:1 CaH_2 to Si molar ratio (Sample 1, Table 2), CaSi is the main decomposition product (89 wt%) along with 7 wt% of $CaSi_2$. Sample 2 (1:2 molar ratio) decomposed predominately in to $CaSi_2$ (74 wt%), which is thermodynamically expected from the HSC predictions, although Si (13 wt%) and CaSi (5 wt%) phases are also present. The most interesting results are reflected for the sample with a 2:1 molar ratio (Sample 3, Table 2). According to thermodynamic predictions, the expected decomposition product should be a Ca_2Si phase. Instead CaH_2 (6 wt%), CaSi (6 wt%) and Ca_5Si_3 (79 wt%) are the observed phases in the decomposed sample. This indicates that a multistep decomposition reaction takes place and the proposed decomposition mechanism of this particular sample is shown in Fig. 2, which was also partially experimentally confirmed by DSC-TGA-MS data (Fig. 3) and *in-situ* SR-XRD (Fig. 4). Five consecutive reactions take place in order to finally produce Ca_2Si. CaH_2 initially reacts with Si to form $CaSi_2$ (RXN 1 in Fig. 2), which then reacts with some of the remaining CaH_2 in the system to form Ca_3Si_4 (RXN 2 in Fig. 2). Ca_3Si_4 then reacts again with CaH_2 to form CaSi (RXN 3 in Fig. 2). The final two steps consist of the reaction between CaSi and CaH_2 to form Ca_5Si_3 (RXN 4 in Fig. 2), which then finally reacts with last remaining CaH_2 in the system to form the Ca_2Si phase (RXN 5 in Fig. 2). According to the XRD data, it appears that the thermal reaction for Sample 3 (2:1) stopped after RXN 4 (in Fig. 2), and therefore CaH_2 and Ca_5Si_3 are present. The final decomposition step did not take place because the equilibrium pressure associated with the final step had already been reached in the system, and that reaction was therefore not thermodynamically favourable. This is also reflected in the observed experimental value of desorbed hydrogen for that sample, which is 16% lower than the theoretically value.

The same observation can be made for Sample 5 (Table 1) with a 5:3 CaH_2 to Si molar ratio, therefore the decomposition products are CaSi (54 wt%), $CaSi_2$ (9 wt%) and Ca_5Si_3 (25 wt%), instead of having only Ca_5Si_3 (RXN5, in Table 1). In contrast, Sample 4 (Table 1), which has a 3:4 molar ratio of CaH_2 to Si has only CaSi (45 wt%) and $CaSi_2$ (49 wt%) phases present after its decomposition at almost equal amounts. The expected decomposition product of that particular reaction is Ca_3Si_4, which is completely absent. According to Manfrinetti et al. fragments of Ca_3Si_4 crystals were observed in their study only after annealing pure Ca and pure Si at 900 °C and then quenched [52]. As quenching is compulsory for the formation of Ca_3Si_4, it means that this phase may not be stable while it cools slowly to room temperature. Hence, it may have potentially changed to the observed phases (CaSi and $CaSi_2$).

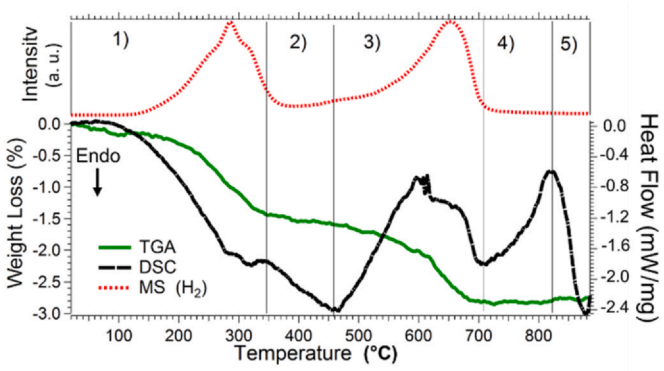

Fig. 3. Differential scanning calorimetry (DSC), thermogravimetric analysis (TGA) and mass spectrometry (MS) data of the $2CaH_2$ and Si system. Temperature ramp = 10 °C/min.

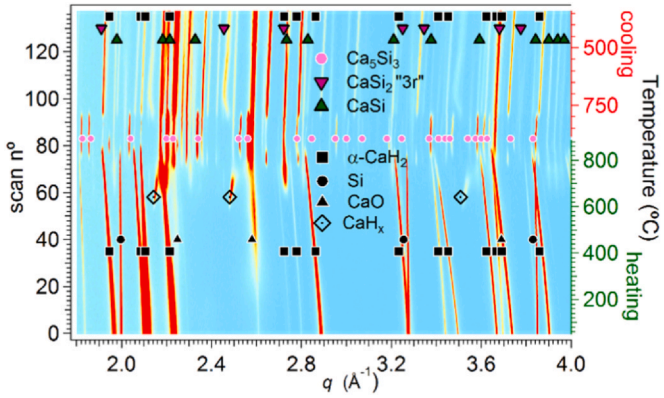

Fig. 4. *In-situ* synchrotron powder diffraction of the $2CaH_2$ and Si system (λ = 0.59027 Å). Heating ramp up to 886 °C (10 °C/min), and cooling ramp down to 338 °C under 1.5 bar H_2 back pressure.

The multistep experimental decomposition pathway (Fig. 2) of the $2CaH_2$ and Si system (Sample 3, Table 2) is also mirrored in the DSC, TGA and MS data presented in Fig. 3. From the TGA curve, it can be seen that more than half (1.5 wt%) of the hydrogen is desorbed before 500 °C. This is due to the first two reaction steps of CaH_2 with Si as proposed in Fig. 2. CaH_2 initially reacts with Si to form $CaSi_2$ (RXN1 in Fig. 2, 0.9 wt% H_2) and then further reacts with $CaSi_2$ to form Ca_3Si_4 (RXN2 in Fig. 2, 0.45 wt% H_2). This observation can be confirmed from the hydrogen peaks detected from the MS data as well as the two endothermic features shown in the DSC curve for this temperature range. Another broad hydrogen peak is detected in the MS data between 600–750 °C, which is also reflected in both the TGA data that corresponds to a 1.16 wt% mass loss and two

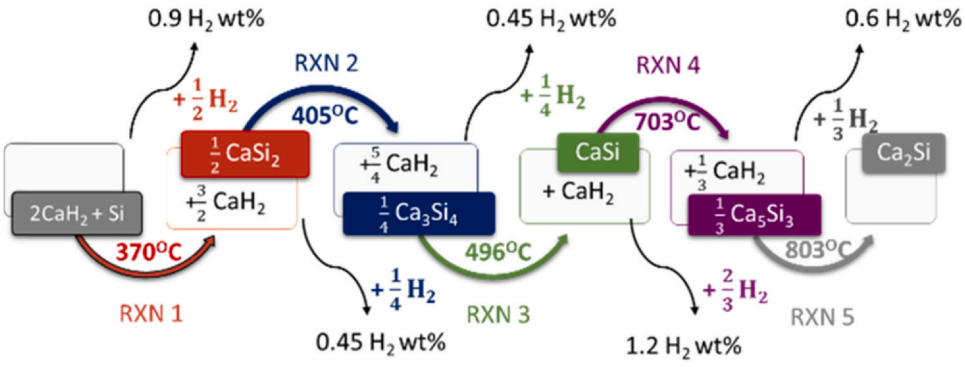

Fig. 2. Proposed decomposition pathway of the $2CaH_2$ and Si system that consists of 5 decomposition steps.

endothermic peaks in the DSC curve. This is due to RXN 3 (in Fig. 2) and RXN 4 (in Fig. 2) taking place in the system between 600–750 °C, whereas RXN5 (in Fig. 2) takes place above 750 °C. According to the TGA data, the total experimental desorbed hydrogen was 2.86 wt%, which is 95% of the theoretical H_2 wt% of this system at 900 °C. According to the phase diagram of Ca-CaH_2, the melting point of CaH_2 depending on the purity varies between 842 °C and 983 °C under 1 bar of H_2 [31]. The last endothermic phase transition present in the DSC curve may be due to Ca or CaH_2 melting under vacuum.

The *in-situ* SR-XRD data illustrated in Fig. 4 for the same system (Sample 3, Table 2) shows a phase transformation of CaH_2 at 600 °C. According to Peterson et al., depending on the quality of calcium hydride, it transforms to a CaH_2-β phase and Ca α, γ or β phase [31]. The q values ($q = 4\pi(sin\theta)/\lambda$) of this observed phase are shifting towards a higher q range with temperature, inferring that the lattice parameters are reducing, while the initial phase of CaH_2 transforms to this observed new phase. The initial formation of Ca_5Si_3 (*I*4/*mcm*) is observed at 780–800 °C in the *in-situ* SR-XRD data, which is also reflected in the DSC-TGA-MS data (Fig. 3), where an endothermic peak is present, together with a step in the weight loss of the system and a peak maxima associated with the hydrogen gas detected at 710 °C, respectively. The difference in temperature is only due to the different conditions applied during the data collection, *i.e.* the SR-XRD data was collected under a H_2 pressure of between 1 and 1.5 bar, therefore supressing the decomposition reaction, whereas the DSC-TGA-MS data was obtained while the sample was under an argon flow (equivalent of dynamic vacuum). CaO phases are present throughout the *in-situ* SR-XRD data, becoming more pronounced when the final temperature is reached and cooling starts. This is mainly due to the corrosion of the quartz capillary from the molten decomposition products causing oxidation of the sample. It is noticeable that as soon as cooling starts, Ca_5Si_3 transforms to CaSi and CaH_2, implying that RXN4 (in Fig. 2) is reversible ($CaH_2 + CaSi \rightleftharpoons 1/3Ca_5Si_3 + 1/3CaH_2 + 2/3H_2$). This reversible reaction is ideal for TES applications since the temperature range in which it occurs is between 600 and 800 °C with pressure close to 1 bar of H_2. In order to confirm this, a series of PCI measurements were conducted to obtain a van't Hoff plot (Fig. 5) and determine the enthalpy of RXN4 in Fig. 2.

Fig. 5 shows the four PCI measurements and the generated van't Hoff plot for the $2CaH_2 + Si$ system (Sample 3) in relation to the desorption reaction between 698 and 778 °C. Initial observations show that the pressure does not reach a flat equilibrium plateau at these four selected temperatures. Ideally, a TES material used in CSP plants should have a flat plateau at their equilibrium pressure both for absorption and desorption, with little hysteresis. As explained by Sheppard et al. a sloping plateau is a disadvantage for engineering, since hydrogen absorption and desorption at a constant pressure and temperature is desired due to the simplicity of the system [19,46]. The slope in this case is attributed to the formation of a CaH_x solid solution. Tortoza et al. have similarly reported a sloping plateau in their PCI curves due to the formation of a $Mg(H_xF_{1-x})_2$ solid solution [16]. The formation of the CaH_x solid solution in the present $2CaH_2 + Si$ system is confirmed by the *in-situ* SR-XRD data (Fig. 4).

From the predicted reaction scheme in Fig. 2, the reaction between CaH_2 and CaSi above 703 °C to form Ca_5Si_3 (RXN 4 in Fig. 2 for the $2CaH_2$ and Si system; when balanced this is RXN 16 in Table 1) should have an enthalpy of reaction; ΔH_{des} = 107.3 kJ mol^{-1} H_2. Using the van't Hoff equation, the experimental ΔH_{des} is 154 ± 4 kJ mol^{-1} H_2 and ΔS_{des} is 151 ± 3 J mol^{-1}. K^{-1} H_2 resulting in a desorption temperature of 747 ± 33 °C at a pressure of 1 bar. The enthalpy and entropy values are higher than the predicted ones. The kinetic data for the PCI measurement at 750 °C (Fig. S2) shows that the equilibrium plateau was not reached after 5 h for each desorption step. Therefore, the pressure is underestimated, which corresponds to an overestimation of the thermodynamic values. The total hydrogen content desorbed during the plateau is 0.80 ± 0.06 wt%, which corresponds to only 2/3 of the theoretical value for RXN4 (in Fig. 2). *Ex-situ* XRD analysis of this sample after the PCI measurement (Fig. S3) shows that this mismatch in the values and is partially due to: (i) the presence of CaO, and (ii) the formation of a solid solution with Ca_5Si_3 not being the only phase in the sample.

As the reaction between CaH_2 and CaSi at ~700 °C forming Ca_5Si_3 (plus residual CaH_2, RXN 4 in Fig. 2) is stable upon cycling, a cost analysis of the material for TES applications was undertaken. To ensure all CaH_2 is consumed during the process the system was evaluated in a ratio of $2CaH_2$:3CaSi. The raw material cost of the HTMH/LTMH system was estimated, using $NaAlH_4$ as the LTMH, determining its overall commercial viability as a TES system. The total raw material cost was estimated to be \$17.38/kWh_{th}, and calculated by taking into consideration that the total practical hydrogen content of the CaH_2 and CaSi system was 0.8 wt% (determined by PCI experiments). The engineering cost of the container and the heat transfer system, as required by the Sunshot's target, was not included in the above cost estimate [27]. Overall, even though the $2CaH_2 + 3CaSi$ system does not meet the \$15/kWh_{th} target (which includes the cost of the: (i) raw material, (ii) engineering of the container and (iii) heat transfer system), it is not entirely ruled out of interest due to its high operating temperatures in the range of 700–850 °C at ≈ 1–5 bar pressure. Also, a less expensive solution than $NaAlH_4$ can be used as a LTMH, such as compressed gas storage, making it a more competitive option.

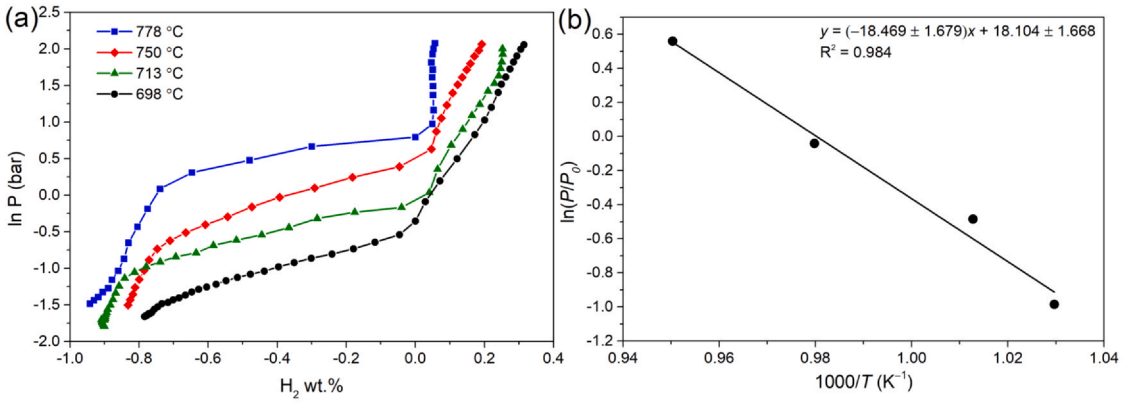

Fig. 5. (a) PCI measurements for $2CaH_2 + Si$ system of the desorption reaction between 698 °C and 778 °C (RXN 4 in Fig. 2, the onset of the desorption plateaus have been shifted to 0 wt% H_2 to allow direct comparison); (b) the generated van't Hoff plot. Equilibrium pressures used for the van't Hoff plot were determined at −0.4 wt% H_2.

4. Conclusions

In the present work, a Ca–Si system was theoretically and experimentally investigated for high-temperature thermochemical energy storage (TES) applications for the next-generation of CSP plants. Temperature programmed desorption (TPD) measurements performed from room temperature up to 750 °C on five selected ratios of CaH_2 and Si (Ca:Si; 1:1, 1:2, 2:1, 3:4 and 5:3) determined that the most suitable sample for such applications was the one with a 2:1 CaH_2 to Si molar ratio (Sample 3). This sample exhibited the highest concentration of experimentally desorbed hydrogen upon heating in comparison to the other samples. Theoretically, it was determined that the reaction between $2CaH_2 + Si$ is multistep in nature with a total of five reactions taking place as temperature increases from room temperature to above 800 °C. These reactions were assessed experimentally by DSC-TGA-MS, XRD and PCI analysis to determine the exact reaction pathway and the thermal properties of the system. At ~700 °C a reaction occurs between CaH_2 and CaSi resulting in the formation of Ca_5Si_3 (and excess CaH_2), releasing 0.8 wt% H_2. PCI analysis determined $\Delta H_{des} = 154 \pm 4\ kJ\ mol^{-1}\ H_2$ and $\Delta S_{des} = 151 \pm 3\ J\ mol^{-1}\ K^{-1}\ H_2$, with the reaction also being determined to be reversible. With an operating temperature of 700–850 °C, and operating pressures of ≈ 1–5 bar H_2, the energy efficiency and modest engineering constraints of the reversible reaction between $2CaH_2$ and 3CaSi forming $Ca_5Si_3 + 2\,H_2$, make this material a potential candidate to be a commercially viable thermal energy storage material for the next generation of CSP plants.

Author contributions

The manuscript was written through contributions of all authors. All authors have given approval to the final version of the manuscript.

CRediT authorship contribution statement

Arnaud C. M. Griffond: Conceptualisation, Methodology, Validation, Formal analysis, Investigation, Data Curation, Writing - Original Draft, Visualization. **M. Veronica Sofianos:** Investigation, Methodology, Formal analysis, Writing - Review & Editing. **Drew A. Sheppard:** Conceptualisation, Investigation, Methodology, Formal analysis, Writing - Review & Editing, Supervision. **Terry D. Humphries:** Investigation, Methodology, Formal analysis, Writing - Review & Editing, Supervision. **Anna-Lisa Sargent:** Investigation, Writing - Review & Editing. **Martin Dornheim:** Investigation, Writing - Review & Editing. **Kondo-Francois Aguey-Zinsou:** Investigation, Writing - Review & Editing. **Craig E. Buckley:** Conceptualisation, Writing - Review & Editing, Resources, Supervision, Project administration, Funding acquisition.

Notes

The authors declare no competing financial interest.

Declaration of competing interest

The authors declare that they have no known competing financial interests or personal relationships that could have appeared to influence the work reported in this paper.

Acknowledgements

CEB, DAS, MVS, and TDH acknowledge the financial support of the Australian Research Council (Australia) for the ARC Linkage grant LP150100730. CEB, MVS and TDH acknowledge the financial support from the Department of Industry Innovation and Science (Australia) for the 2019 Global Innovation Linkage (GIL73589) grant. MVS acknowledges the financial support of the University College Dublin (Ireland) for the Ad Astra fellowship, and DAS acknowledges the financial support of Curtin University (Australia) for the Postdoctoral Research Fellowship. CEB, MVS, DAS, ACMG, TDH, A-LS and MD acknowledge financial support of the Australia-Germany Joint Research Cooperation Scheme DAAD (Project 57218310). CEB acknowledges the financial support of the Australian Research Council for the ARC LIEF grants LE0775551 and LE0989180, which enabled the TPD and PCI measurements to be undertaken. The *in-situ* synchrotron powder diffraction data was collected on the Powder Diffraction beamline at the Australian Synchrotron, part of ANSTO.

Appendix A Supporting information

Supplementary data associated with this article can be found in the online version at doi:10.1016/j.jallcom.2020.158229.

References

[1] D. Abbott, Keeping the energy debate clean: how do we supply the world's energy needs? Proc. IEEE 98 (2010) 42–66, https://doi.org/10.1109/jproc.2009.2035162
[2] Concentrating Solar Power Projects. ⟨https://solarpaces.nrel.gov/⟩. Accessed August 19, 2020.
[3] Renewables 2016 Global Status Report. ⟨http://www.ren21.net/wp-content/uploads/2016/05/GSR_2016_Full_Report_lowres.pdf⟩. Accessed 08/02/2019.
[4] S. Kaneff, Viable distributed dish central plant solar power: status, new developments, potential, J. Phys. IV (9) (1999) 195–200, https://doi.org/10.1051/jp4:1999329
[5] B. Kongtragool, S. Wongwises, A review of solar-powered Stirling engines and low temperature differential Stirling engines, Renew. Sustain. Energy Rev. 7 (2003) 131–154, https://doi.org/10.1016/S1364-0321(02)00053-9
[6] L.C. Spencer, A comprehensive review of small solar-powered heat engines: Part I. A history of solar-powered devices up to 1950, Solar Energy 43 (1989) 191–196, https://doi.org/10.1016/0038-092X(89)90019-4
[7] I. Dincer, M.A. Rosen, Thermal Energy Storage: Systems and Applications, Second ed., John Wiley & Sons Ltd, New York, United States, 2010 978-0-470-74706-3.
[8] M. Medrano, A. Gil, I. Martorell, X. Potau, L.F. Cabeza, State of the art on high-temperature thermal energy storage for power generation. Part 2-Case studies, Renew. Sustain. Energy Rev. 14 (2010) 56–72, https://doi.org/10.1016/j.rser.2009.07.036
[9] R. Jacob, F. Bruno, Review on shell materials used in the encapsulation of phase change materials for high temperature thermal energy storage, Renew. Sustain. Energy Rev. 48 (2015) 79–87, https://doi.org/10.1016/j.rser.2015.03.038
[10] U. Pelay, L.A. Lu, Y.L. Fan, D. Stitou, M. Rood, Thermal energy storage systems for concentrated solar power plants, Renew. Sustain. Energy Rev. 79 (2017) 82–100, https://doi.org/10.1016/j.rser.2017.03.139
[11] P. Pardo, A. Deydier, Z. Anxionnaz-Minvielle, S. Rouge, M. Cabassud, P. Cognet, A review on high temperature thermochemical heat energy storage, Renew. Sustain. Energy Rev. 32 (2014) 591–610, https://doi.org/10.1016/j.rser.2013.12.014
[12] D.N. Harries, M. Paskevicius, D.A. Sheppard, T.E.C. Price, C.E. Buckley, Concentrating solar thermal heat storage using metal hydrides, Proc. IEEE 100 (2012) 539–549, https://doi.org/10.1109/Jproc.2011.2158509
[13] T.D. Humphries, K.T. Moller, W.D.A. Rickard, M.V. Sofianos, S.M. Liu, C.E. Buckley, M. Paskevicius, Dolomite: a low cost thermochemical energy storage material, J. Mater. Chem. A 7 (2019) 1206–1215, https://doi.org/10.1039/c8ta07254j
[14] T.D. Humphries, D.A. Sheppard, G.Q. Li, M.R. Rowles, M. Paskevicius, M. Matsuo, K.F. Aguey-Zinsou, M.V. Sofianos, S. Orimo, C.E. Buckley, Complex hydrides as thermal energy storage materials: characterisation and thermal decomposition of $Na_2Mg_2NiH_6$, J. Mater. Chem. A 6 (2018) 9099–9108, https://doi.org/10.1039/c8ta00822a
[15] T.D. Humphries, D.A. Sheppard, M.R. Rowles, M.V. Sofianos, C.E. Buckley, Fluoride substitution in sodium hydride for thermal energy storage applications, J. Mater. Chem. A 4 (2016) 12170–12178, https://doi.org/10.1039/c6ta03623f
[16] M.S. Tortoza, T.D. Humphries, D.A. Sheppard, M. Paskevicius, M.R. Rowles, M.V. Sofianos, K.F. Aguey-Zinsou, C.E. Buckley, Thermodynamics and performance of the Mg–H–F system for thermochemical energy storage applications, Phys. Chem. Chem. Phys. 20 (2018) 2274–2283, https://doi.org/10.1039/c7cp07433f
[17] K.T. Møller, A. Ibrahim, C. Buckley, M. Paskevicius, Inexpensive thermochemical energy storage utilising additive enhanced limestone, J. Mater. Chem. A 8 (2020) 9646–9653, https://doi.org/10.1039/D0TA03080E
[18] K.T. Møller, D.A. Sheppard, D. Ravnsbæk, C.E. Buckley, E. Akiba, H.-W. Li, T.R. Jensen, Complex metal hydrides for hydrogen, thermal and electrochemical energy storage, Energies 10 (2017) 1645, https://doi.org/10.3390/en10101645
[19] D.A. Sheppard, C. Corgnale, B. Hardy, T. Motyka, R. Zidan, M. Paskevicius, C.E. Buckley, Hydriding characteristics of NaMgH2F with preliminary technical

and cost evaluation of magnesium-based metal hydride materials for concentrating solar power thermal storage, RSC Adv. 4 (2014) 26552–26562, https://doi.org/10.1039/c4ra01682c
[20] D.A. Sheppard, M. Paskevicius, T.D. Humphries, M. Felderhoff, G. Capurso, J.B. von Colbe, M. Dornheim, T. Klassen, P.A. Ward, J.A. Teprovich, C. Corgnale, R. Zidan, D.M. Grant, C.E. Buckley, Metal hydrides for concentrating solar thermal power energy storage, Appl. Phys. A 122 (2016) 395, https://doi.org/10.1007/s00339-016-9825-0
[21] K. Manickam, P. Mistry, G. Walker, D. Grant, C.E. Buckley, T.D. Humphries, M. Paskevicius, T. Jensen, R. Albert, K. Peinecke, M. Felderhoff, Future perspectives of thermal energy storage with metal hydrides, Int. J. Hydrogen Energy 44 (2019) 7738–7745, https://doi.org/10.1016/j.ijhydene.2018.12.011
[22] P.A. Ward, C. Corgnale, J.A. Teprovich, T. Motyka, B. Hardy, D. Sheppard, C. Buckley, R. Zidan, Technical challenges and future direction for high-efficiency metal hydride thermal energy storage systems, Appl. Phys. A 122 (2016) 462, https://doi.org/10.1007/s00339-016-9909-x
[23] Y. Tian, C.Y. Zhao, A review of solar collectors and thermal energy storage in solar thermal applications, Appl. Energy 104 (2013) 538–553, https://doi.org/10.1016/j.apenergy.2012.11.051
[24] R. Sioshansi, P. Denholm. The Value of Concentrating Solar Power and Thermal Energy Storage, Technical Report NREL-TP-6A2-45833.; NREL: (2010).
[25] D.A. Sheppard, C.E. Buckley, The potential of metal hydrides paired with compressed hydrogen as thermal energy storage for concentrating solar power plants, Int. J. Hydrogen Energy 44 (2019) 9143–9163, https://doi.org/10.1016/j.ijhydene.2019.01.271
[26] C. Corgnale, B. Hardy, T. Motyka, R. Zidan, J. Teprovich, B. Peters, Screening analysis of metal hydride based thermal energy storage systems for concentrating solar power plants, Int. J. Hydrogen Energy 38 (2014) 821–833, https://doi.org/10.1016/j.rser.2014.07.049
[27] SunShot Vision Study, Chapter 5: Concentrating Solar Power: Technologies, Cost, and Performance, US Department of Energy: US Department of Energy, 2012, pp. 97–123.
[28] M.V. Sofianos, S. Randall, M. Paskevicius, K.F. Aguey-Zinsou, M.R. Rowles, T.D. Humphries, C.E. Buckley, Exploring halide destabilised calcium hydride as a high-temperature thermal battery, J. Alloys Compd. 819 (2020) 153340, https://doi.org/10.1016/j.jallcom.2019.153340
[29] M. Hirscher, V.A. Yartys, M. Baricco, J.B. von Colbe, D. Blanchard, R.C. Bowman, D.P. Broom, C.E. Buckley, F. Chang, P. Chen, Y.W. Cho, J.C. Crivello, F. Cuevas, W.I.F. David, P.E. de Jongh, R.V. Denys, M. Dornheim, M. Felderhoff, Y. Filinchuk, G.E. Froudakis, D.M. Grant, E.M. Gray, B.C. Hauback, T. He, T.D. Humphries, T.R. Jensen, S. Kim, Y. Kojima, M. Latroche, H.W. Li, M.V. Lototskyy, J.W. Makepeace, K.T. Moller, L. Naheed, P. Ngene, D. Noreus, M.M. Nygard, S.I. Orimo, M. Paskevicius, L. Pasquini, D.B. Ravnsbaek, M.V. Sofianos, T.J. Udovic, T. Vegge, G.S. Walker, C.J. Webb, C. Weidenthaler, C. Zlotea, Materials for hydrogen-based energy storage - past, recent progress and future outlook, J. Alloys Compd. 827 (2020) 153548, https://doi.org/10.1016/j.jallcom.2019.153548
[30] M. Wang, W.H. Sun, C.S. Sha, B. Hu, Y. Du, L.X. Sun, H.H. Xu, J.C. Wang, S.H. Liu, Thermodynamic modeling of the Li–H and Ca–H systems, J. Phase Equilib. Diffus. 33 (2012) 89–96, https://doi.org/10.1007/s11669-012-9997-z
[31] D. Peterson, V. Fattore, Calcium-calcium hydride phase system, J. Phys. Chem. 65 (1961) 2062–2064, https://doi.org/10.1021/j100828a034
[32] R.W. Curtis, P. Chiotti, Thermodynamic properties of calcium hydride1, J. Phys. Chem. 67 (1963) 1061–1065, https://doi.org/10.1021/j100799a027
[33] J.J. Vajo, G.L. Olson, Hydrogen storage in destabilized chemical systems, Scr. Mater. 56 (2007) 829–834, https://doi.org/10.1016/j.scriptamat.2007.01.002
[34] E. Veleckis, Application of the hydrogen titration method to a thermodynamic investigation of solid Al–Ca alloys, J. Less Common Metals 80 (1981) 241–255, https://doi.org/10.1016/0022-5088(81)90098-9
[35] P.A. Ward, J.A. Teprovich, Y.F. Liu, J. He, R. Zidan, High temperature thermal energy storage in the $CaAl_2$ system, J. Alloys Compd. 735 (2018) 2611–2615, https://doi.org/10.1016/j.jallcom.2017.10.191
[36] L. Wöhler, F. Müller, Uber die Calciumsilicide, Z Anorg. Allg. Chem. 120 (1921) 49–70, https://doi.org/10.1002/zaac.19211200106
[37] E.Y. Anikina, V.N. Verbetsky, Investigation of hydrogen desorption from CaSiH by means of calorimetric method, J. Therm. Anal. Calorim. 118 (2014) 801–805, https://doi.org/10.1007/s10973-014-3920-2
[38] H. Wu, W. Zhou, T.J. Udovic, J.J. Rush, T. Yildirim, Structural variations and hydrogen storage properties of Ca5Si3 with Cr5B3-type structure, Chem. Phys. Lett. 460 (2008) 432–437, https://doi.org/10.1016/j.cplett.2008.06.018
[39] H. Wu, W. Zhou, T.J. Udovic, J.J. Rush, Hydrogen storage in a novel destabilized hydride system, Ca_2SiH_x: effects of amorphization, Chem. Mater. 19 (2007) 329–334, https://doi.org/10.1021/cm062274c
[40] Outukumpu HSC Chemistry, 6.1; Chemistry Software: Houston, 2006.
[41] A.T. Dinsdale, SGTE data for pure elements, Calphad Comput. Coupling Phase Diagr. Thermochem. 15 (1991) 317–425, https://doi.org/10.1016/0364-5916(91)90030-N
[42] M. Binnewies, E. Milke, Thermochemical Data of Elements and Compounds, Wiley-VCH, 1999.
[43] M. Heyrman, P. Chartrand, Thermodynamic evaluation and optimization of the Ca–Si system, J. Phase Equilib. Diffus. 27 (2006) 220–230, https://doi.org/10.1361/154770306×109755
[44] H. Rietveld, A profile refinement method for nuclear and magnetic structures, J. Appl. Crystallogr. 2 (1969) 65–71, https://doi.org/10.1107/S0021889869006558
[45] M. Paskevicius, D.A. Sheppard, C.E. Buckley, Thermodynamic changes in mechanochemically synthesized magnesium hydride nanoparticles, J. Am. Chem. Soc. 132 (2010) 5077–5083, https://doi.org/10.1021/ja908398u
[46] D.A. Sheppard, M. Paskevicius, P. Javadian, I.J. Davies, C.E. Buckley, Methods for accurate high-temperature Sieverts-type hydrogen measurements of metal hydrides, J. Alloys Compd. 787 (2019) 1225–1237, https://doi.org/10.1016/j.jallcom.2019.02.067
[47] K.S. Wallwork, B.J. Kennedy, D. Wang, The high resolution powder diffraction beamline for the Australian Synchrotron, Synchrotron Radiation Instrumentation, Pts 1 and 2, 879, 879–882, 2007.
[48] B. Schmitt, C. Bronnimann, E.F. Eikenberry, F. Gozzo, C. Hormann, R. Horisberger, B. Patterson. Mythen detector system Nuclear Instruments and Methods in Physics Research Section A: Accelerators, Spectrometers, Detectors and Associated Equipment, 501, 267–272, 2003. doi: 10.1016/S0168-9002(02)02045-4.
[49] P.D. Pathak, N.G. Vasavada, Thermal expansion of NaCl, KCl and CsBr by X-ray diffraction and the law of corresponding states, Acta Crystallogr. A 26 (1970) 655–658, https://doi.org/10.1107/s0567739470001602
[50] I.-K. Suh, H. Ohta, Y. Waseda, High-temperature thermal expansion of six metallic elements measured by dilatation method and X-ray diffraction, J. Mater. Sci. 23 (1988) 757–760, https://doi.org/10.1007/bf01174717
[51] B.R.S. Hansen, K.T. Moller, M. Paskevicius, A.C. Dippel, P. Walter, C.J. Webb, C. Pistidda, N. Bergemann, M. Dornheim, T. Klassen, J.E. Jorgensen, T.R. Jensen, In situ X-ray diffraction environments for high-pressure reactions, J. Appl. Crystallogr. 48 (2015) 1234–1241, https://doi.org/10.1107/S1600576715011735
[52] P. Manfrinetti, M.L. Fornasini, A. Palenzona, The phase diagram of the Ca–Si system, Intermetallics 8 (2000) 223–228, https://doi.org/10.1016/S0966-9795(99)00112-0